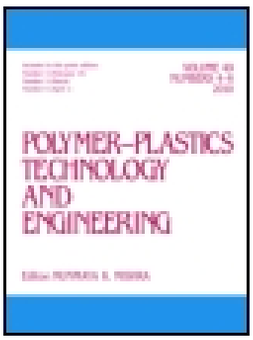

Taylor & Francis
Taylor & Francis Group

Polymer-Plastics Technology and Engineering

ISSN: 0360-2559 (Print) 1525-6111 (Online) Journal homepage: http://www.tandfonline.com/loi/lpte20

Millimeter wave absorbing property of flexible graphene/acrylonitrile-butadiene rubber composite in 5G frequency band

Yukun Chen, Xingfeng Fu, Lie Liu, Ying Zhang, Liming Cao, Daosheng Yuan & Pingan Liu

To cite this article: Yukun Chen, Xingfeng Fu, Lie Liu, Ying Zhang, Liming Cao, Daosheng Yuan & Pingan Liu (2018): Millimeter wave absorbing property of flexible graphene/acrylonitrile-butadiene rubber composite in 5G frequency band, Polymer-Plastics Technology and Engineering, DOI: 10.1080/03602559.2018.1542714

To link to this article: https://doi.org/10.1080/03602559.2018.1542714

Published online: 05 Nov 2018.

Submit your article to this journal

Article views: 27

View Crossmark data

Full Terms & Conditions of access and use can be found at
http://www.tandfonline.com/action/journalInformation?journalCode=lpte20

POLYMER-PLASTICS TECHNOLOGY AND ENGINEERING
https://doi.org/10.1080/03602559.2018.1542714

Taylor & Francis
Taylor & Francis Group

Check for updates

Millimeter wave absorbing property of flexible graphene/acrylonitrile-butadiene rubber composite in 5G frequency band

Yukun Chen[a], Xingfeng Fu[a], Lie Liu[b,c], Ying Zhang[b], Liming Cao[a], Daosheng Yuan[a], and Pingan Liu[d]

[a]Lab of Advanced Elastomer, School of Mechanical & Automotive Engineering, South China University of Technology, Guangzhou, China; [b]Shenzhen General Test Systems, Shenzhen, China; [c]College of Electrical and Information Engineering, Hunan University, Changsha, China; [d]School of Materials Science and Engineering, South China University of Technology, Guangzhou, China

ABSTRACT

The coming fifth generation mobile communication technology (5G) puts forward enormous requirements on millimeter wave (MMW) absorbing materials above 24 GHz. In the present work, elastic absorbing composites were fabricated with reduced graphene oxide (RGO) of different reduction time and nitrile rubber (NBR). A series of characterization methods were used to study the reduction degree and the structure of composites, the electromagnetic parameters of composites in 26.5–40 GHz were also measured and used to conduct an analytical computation of reflection loss (RL). It was found that, 3h-RGO/NBR presented the minimum RL of −45 dB at 35.4 GHz while 7h-RGO/NBR exhibited the widest effective bandwidth (<-10 dB) about 6.5 GHz. In addition, the mechanical properties of composites were also improved by RGO. Therefore, the obtained RGO/NBR composites displayed promising prospect as elastic MMW absorbing materials for 5G applications.

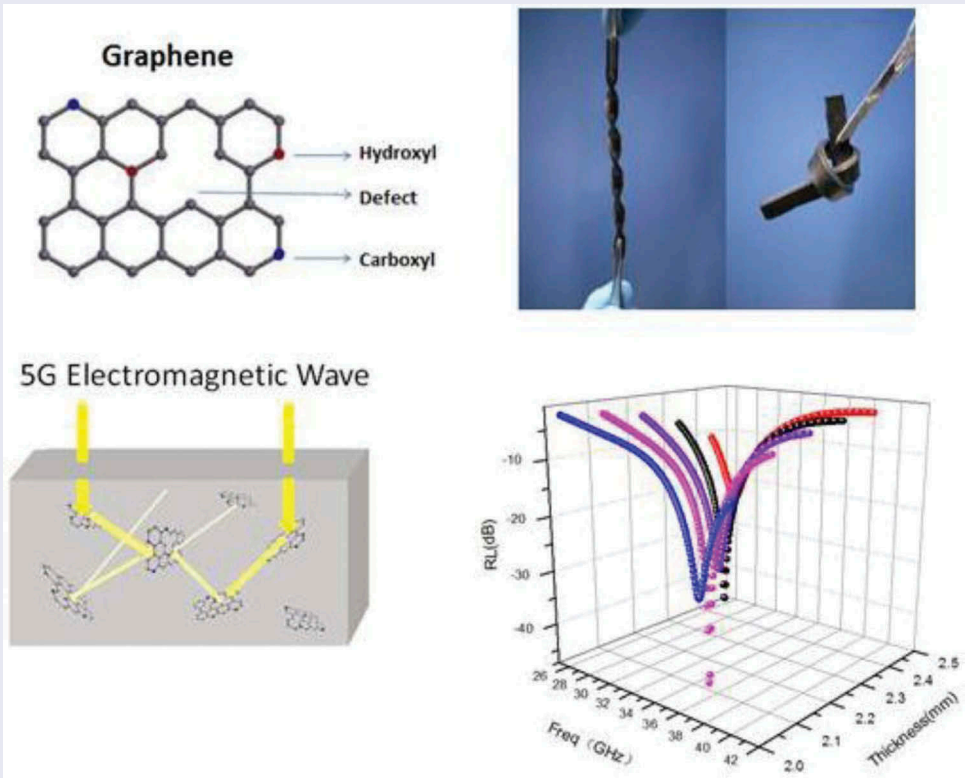

ARTICLE HISTORY
Received 18 May 2018
Revised 18 September 2018
Accepted 27 October 2018

KEYWORDS
Nitrile rubber; reduced graphene oxide; millimeter wave absorbing; 5G Frequency Band

CONTACT Yukun Chen cyk@scut.edu.cn Lab of Advanced Elastomer, South China University of Technology, Guangzhou, China; Pingan Liu paliu@scut.edu.cn School of Materials Science and Engineering, South China University of Technology, Guangzhou, China

Color versions of one or more of the figures in the article can be found online at www.tandfonline.com/lpte.

© 2018 Taylor & Francis

1. Introduction

The widespread use of electromagnetic (EM) wave in communication industry and electronic devices has brought us much convenience.[1] However, it also accompanies with severe electromagnetic pollutions, such as the interference on operation of electronic devices and the damage on human health, *etc.*[2,3] Therefore, different methods have been developed to solve the problem. Among these methods, electromagnetic interference shielding and electromagnetic wave absorbing are the two most important ones. The former could act as a barrier to elude the EM wave, which doesn't really eliminate the pollution source, but leads to a second pollution in some way. While the later, electromagnetic wave absorbing, is an effective alternative. It can dramatically weak the EM wave by converting EM energy into thermal energy or eliminating it by destructive interference. Because of the outstanding advantages of electromagnetic wave absorbing, it has attracted much attention in recent years.[4] In general, it is desirable that microwave absorption materials with light weight, strong absorption and broad absorbing bandwidth.[5] With the rapid development of wireless communication, the fifth generation mobile communication technology (5G) is around the corner. According to the *RSPG Second Opinion on 5G networks* from European Commission, the high frequency band above 24 GHz will be the pioneer band in Europe to give ultra-high capacity for innovative new services, enabling new business models and sectors of the economy to benefit from 5G.[6] New available frequency bands will certainly bring forward huge demand for corresponding absorbing materials.

In general, microwave absorption materials can be divided into coated and structural ones according to the forming process and carrying capacity. Compared with the former, the later can not only overcome shortcomings such as bad adhesion and large density, but also provide higher bearing capacity and wider absorbing frequency band. [7,8] Structural absorption materials usually consist of two parts, one is matrix, and the other is microwave absorbents. The matrix mainly includes rigid plastics and/or flexible rubbers, and the rubber-based absorbing materials show better prospects of deformability, elasticity and self-healing capacity, etc. [9–14] Microwave absorbents include dielectric style, magnetic style and the complex of both styles. [15–20] Dielectric absorber works through the interaction with electric field or dielectric polarization relaxation, while the magnetic material functions largely by the nature resonance and magnetic loss. For example, Zhai et al. compared different kinds of composites prepared with carbonaceous absorbents and hydrogenated acrylonitrile-butadiene rubber (HNBR).[21] The minimum RL of multi-walled carbon nanotubes (MWCNT)/HNBR (10/100) composite in 2–18 GHz was −49.3 dB, and its −10 dB absorption bandwidth was 3.8 GHz. The corresponding values of conductive carbon black (CCB)/HNBR were −13.1 dB and 2.9 GHz, while the minimum RL of carbon fiber (CF)/HNBR was just −7.1 dB. The obvious differences may result from diminishing increase rate of electrical conductivity and complex permittivity from MWCNT, CCB to CF. Flaifel et al. reported a composite of 12 wt% Ni-Zn ferrite nanoparticles and thermoplastic natural rubber (TPNR), which reached the minimum RL of −38.3 dB at 9.6 GHz with 7 mm thickness.[22]

Over the past decades, extensive studies have been conducted to develop rubber-based microwave absorbing materials with magnetic or multiple absorbents, while most of them are too heavy or rigid to be used widely.[23,24] Moreover, there are relatively less research about flexible rubber-based dielectric absorbing materials, especially when graphene is taken as the absorbent.

NBR has high oil resistance and flexibility, due to which it can be easily used in devices with complex structure and harsh condition like chemical factory. It also has broad applications in the airborne system for its fabulous thermal stability in the range of −20°C to 125°C. Graphene is an excellent dielectric absorbent and possesses excellent properties like light weight, strong electrical and absorption property, etc. Some research on RGO/NBR composites have been carried out in recent years. For example, Ahmed A. Al-Ghamdi et al. fabricated lightweight and flexible acrylonitrile butadiene rubber/graphene nanosheets (NBR/GN) nanocomposites and found that, the nanocomposites can provide a high SE around 77 dB at just 4% CN loading in the frequency range from 1 GHz to 12 GHz.[25] Vivek K. Singh et al. prepared RGO/NBR composite with 10 wt% RGO with layered and porous structure, and the minimum RL can reach −57 dB over a wide frequency range of 7.5–12 GHz. The main absorbing mechanism was explained as the multiple reflections from the dihedral angles formed by the stacks of flakes of RGO sheets.[26]

However, the existing research about RGO/NBR composites is mainly focused on 2–18 GHz, and unable to meet the requirements in the 5G high frequency band. In addition, to the best of our knowledge, the connection between reduction time and microwave absorbing property of RGO/NBR composites has rarely been reported.

In this paper, we prepared composites with NBR and RGO in different reduction time, and studied the absorption property in 26.5–40 GHz for the first time. Besides, the relationship between the microwave absorption and reduction time was also discussed in detail. The results indicated that 3h-RGO/NBR presented the minimum RL value of

−45 dB at 35.4 GHz with 2.1 mm thickness, 5h-RGO/NBR reached the minimum RL of −42.5 dB at 26.8 GHz while the 7h-RGO/NBR achieved the minimum RL of −38.5 dB at 28 GHz and exhibited the widest effective bandwidth of absorption (<-10 dB) about 6.5 GHz. In addition, they also manifested outstanding mechanical properties. Therefore, RGO/NBR composites prepared in this paper are ideal absorbing materials for 5G high frequency bands, which may be used in OTA test system, dark room or other relevant electronic devices, etc.

2. Experimental

2.1. Materials

Graphite oxide (GO) (SE2430W, solid content, 42.7 wt%) was purchased from the Sixth Element (Changzhou) Materials Technology Co.,Ltd. Acrylonitrile–butadiene rubber (NBR3365; acrylonitrile content, 33%) was obtained from NANTEX Industry. Dicumyl peroxide (DCP) was purchased from Sinopharm Chemical Reagent and used as vulcanizing agent. Hydrazine hydrate (80%) was reducing agent and obtained from FuYu Fine Chemical Co., Ltd, and Dimethyl Formamide (DMF; anhydrous, 99%) was supplied by Richjoint. All the chemicals were of analytical grade and used without further purification.

2.2. Preparation of RGO

Firstly, GO was exfoliated acoustically using ultrasonic bath with a power of 100 W in DMF at 1g/150ml for 3 h. Then hydrazine hydrate was subsequently added to the obtained dispersions to trigger the reductive reaction, which carried out in oil bath at 90°C for 3, 5 h and 7 h, respectively.[27] Stirring was used throughout the whole preparation process. The suspension gradually changed its color from brown to black. Then, the suspension was isolated via filtration, washed with distilled water for three times to remove the residual solvent and then dried at 60°C for 48 h. The obtained black powders were named as 3h-RGO, 5h-RGO and 7h-RGO in accordance with the reduction time and preserved for further studies.

2.3. Preparation of RGO/NBR composites

RGO/NBR composites were prepared by solution blending. The desired weight of NBR was dissolved in DMF (1g/20ml) at 90°C, while the predetermined amount of GO was dispersed in DMF (1g/150ml) and exfoliated by bath sonication of 100 W for 2 h. Then, the solution of NBR was added into the GO suspension to make homogeneous slurry under stirring and sonication for 1 h. Reduction reaction was carried out by hydrazine hydrate under same condition as above. The obtained mixture was poured into ice deionized water and yielded black precipitate, which was then dried at 60°C for 24 h. A two-roll mill with a nip clearance of 1 mm was used to compound the dried mixture and 3 wt% DCP at room temperature. The next step was vulcanization that proceeded in an electrically heated compression-molding hydraulic press, where composites were heated and vulcanized under 3 MPa at 170°C for certain time. Finally, the materials were cut into rectangles of 7.15 mm*3.60 mm for waveguide measurements in 26.5–40 GHz. The samples with different reduction time of 3, 5 and 7 h were named as 3h-RGO/NBR, 5h-RGO /NBR and 7h-RGO/NBR, respectively.

2.4. Characterization methods

Fourier transform infrared (FT-IR) spectra of composites were recorded by a Tensor 27 sectrometer (Bruker, Germany) under the attenuated total reflectance (ATR) model (32 consecutive scans and resolution of 4 cm^{-1} wavenumber). Raman spectra were taken on a SENTERRA R200 Raman spectrometer with a 633 nm laser excitation. The crystalline structural of samples was identified by X-ray Diffraction (XRD, D/MAX-III, Japan) using Cu K_α radiation. The scanning rate was 0.02°/s in diffraction angle from 5° to 35° (2θ). X-ray photoelectron spectroscopy (XPS) was conducted using Kratos Axis Ulra DLD spectrometer. The morphology and microstructure of RGO and RGO/NBR composites were investigated by Field-emission scanning electron microscopy (FESEM, Zeiss Merlin, Germany), scanning electron microscopy (SEM, LEO1530VP, Zeiss, Germany) and transition electron microscopy (TEM, Tecnai F30G2; FEI, Eindhoven, Netherlands). The measurement of electromagnetic parameters of RGO/NBR composites was conducted by vector network analyzer (PNA-N5244A) at the frequency range of 26.5–40 GHz with waveguide method. Stress −strain behaviors were carried out on a UT-2080 (U-CAN) instrument under a tensile mode with a crosshead speed of 500 mm/min.

3. Results and discussion

3.1. Characterization of RGO

FT-IR spectra of GO and RGO with different reduction time are shown in Figure 1a. The spectrum of GO illustrates the presence of oxygen-containing groups at 1720, 1232 and 1045 cm^{-1}, which are attributed to

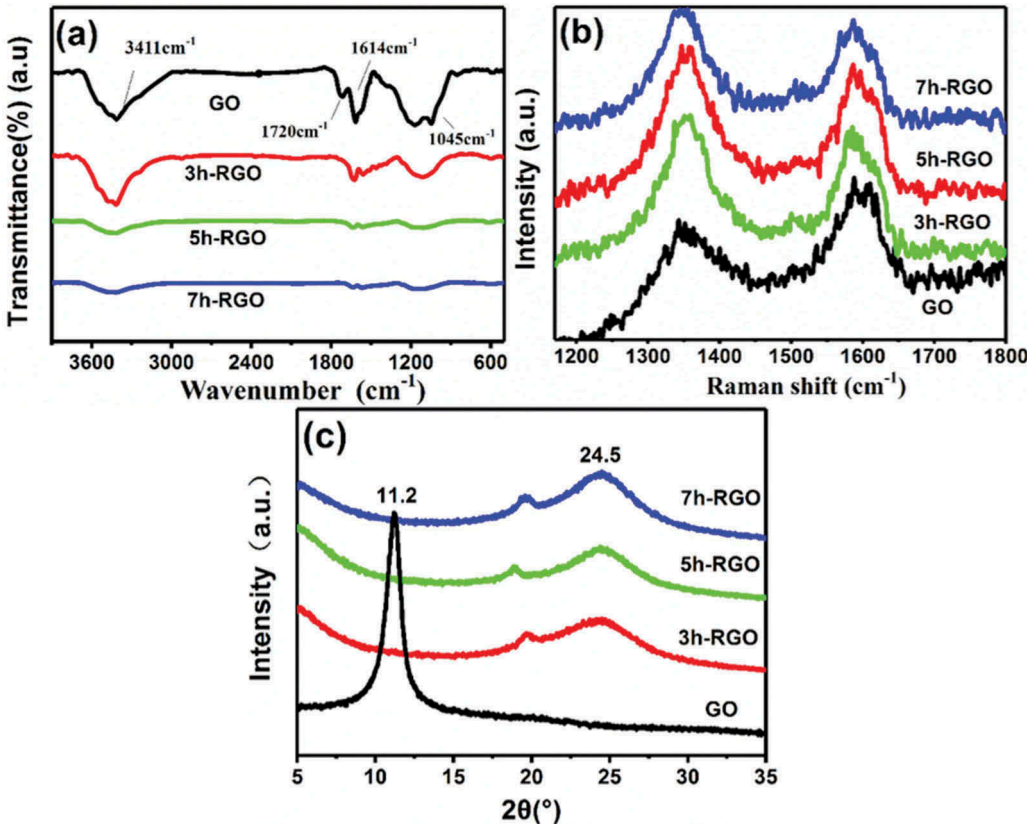

Figure 1. Spectra of (a) FT-IR, (b) Raman and (c) XRD of GO and RGO with different reduction time.

C = O stretching, C-O-C epoxy symmetrical ring deformation and O–H deformation vibration, respectively. The peak at 1402 cm^{-1} is assigned to the C–O–H deformation, and the broad absorption bands at 3411 and 1614 cm^{-1} are attributed to the vibration of water molecules.[28] It is seen that the peaks at 1720 and 1402 cm^{-1} almost disappeared after 3 h reduction, while other characteristic peaks are gradually decreased with increasing the reduction time. All peaks show almost no change when the GO was reduced beyond 5 h, which results in two similar lines of 5h-RGO and 7h-RGO in Figure 1a. The attenuation percent of characteristic peaks were calculated by peak areas and given in Table 1, proving the reduction degree is positively correlated with the reduction time.

Figure 1b shows the result of Raman spectra, where the GO and the RGO in different reduction time are compared. All samples display D-peak at 1357 cm^{-1}, which represents the breathing modes of rings or K-point phonons of A_{1g} symmetry, indicating the structural imperfections caused by defects and functional groups. The G-peak at 1580 cm^{-1} is associated with the first order scattering of E_{2g} mode, representing the sp2 hybridized carbon-carbon bonds.[29,30] The peak area ratios of D band and G band were calculated, i.e. 1.08, 1.41, 1.50, and 1.56 for GO, 3h-RGO, 5h-RGO and 7h-RGO respectively, which increased with the reduction time. This phenomenon could be explained by (i) increased amount of "unorganized" carbon in the samples and (ii) decrease in the graphite crystal size (the sp2 hybridized carbon-carbon bonds).[31]

As shown in Figure 1c, XRD pattern of GO exhibits a sharp single peak at 11.2° corresponding to an interlayer spacing of 7.85 Å, which is due to the oxygen functional groups of GO as well as water molecules held in the interlayer galleries.[32] In the XRD patterns of RGO (agglomerated into a powder form) with

Table 1. The attenuation percent of several characteristic peaks.

		The attenuation percent after different reduction time			
Oxygen-containing group	Position/cm^{-1}	GO	3 h	5 h	7 h
O-H stretching	3411	0	23.4%	80.2%	83.8%
O-H deformation	1621	0	37%	85.4%	89.3%
C-O-C stretching	1041	0	53.5%	86.2%	86.5%

different reduction time, three similar broad peaks are observed at about 24.5° with an interlayer spacing of about 3.7 Å, which is quite close to the (002) graphite peak at 26.5°.[33] The broad peaks at 24.5° could be attributed to the small sheet size, relatively short ordered domains and turbostratic arrangement of RGO, which is confirmed by Raman spectra. In addition, there is a little shoulder peak at 19.8° induced by a bimodal or multimodal character of the interlayer spacing of RGO being not exfoliated perfectly.[34]

The C1s XPS spectra of GO and RGO with different reduction time were used to analyze the diverse chemical environment of carbon atoms, detailed results are depicted in Figure 2. The various peaks at 284.6, 286.1, 287.1 and 288.7 ev correspond to C = C/C-C in aromatic, C-O from epoxy and hydroxyl, C = O in carbonyl and O-C = O from carboxyl groups respectively.[30] After being reduced for different times, the relative intensity of C-O group, which is the main oxygen-containing group in carbonaceous materials, decreased obviously. Compared with the peak values of GO, the value of C = O and O-C = O of RGO also decreased with reduction time and almost approached 0, while the C-O/C = O increased inversely. In addition, the C/O ratios of samples also show an obvious change, where the C/O ratio of GO is 2.34, whereas that of RGO are 7.34, 8.88, and 10.75, respectively. The change could be attributed to the remove of more oxygen-containing groups with increasing reduction time. All these results indicate a gradually increased reduction degree with extending reduction time.

3.2. Microstructure

Figure 3 illustrates the SEM images of RGO samples with different reduction time magnified at 5000 times and 2000 times, which show different structure of these materials. From Figure 3, it is easy to find that wrinkled flakes increased gradually with increasing reduction time, suggesting the increased reduction degree.[35] In addition, it could be clearly noticed that more and more fragments were created with increased reduction time because of overexposure to ultrasonic and velocity mixing stirring. During the preparation process, more oxygen-containing functional groups concealed between sheets were exposed to hydrazine hydrate in solution and got reduced, which is another reason for 7h-RGO achieved the highest reduction degree.

Figure 4a is the TEM image of 7h-RGO/NBR, which shows a homogeneous dispersion of RGO sheet in NBR matrix. The small and light areas marked by white arrows represent both monolayer and few-layer graphene sheets,

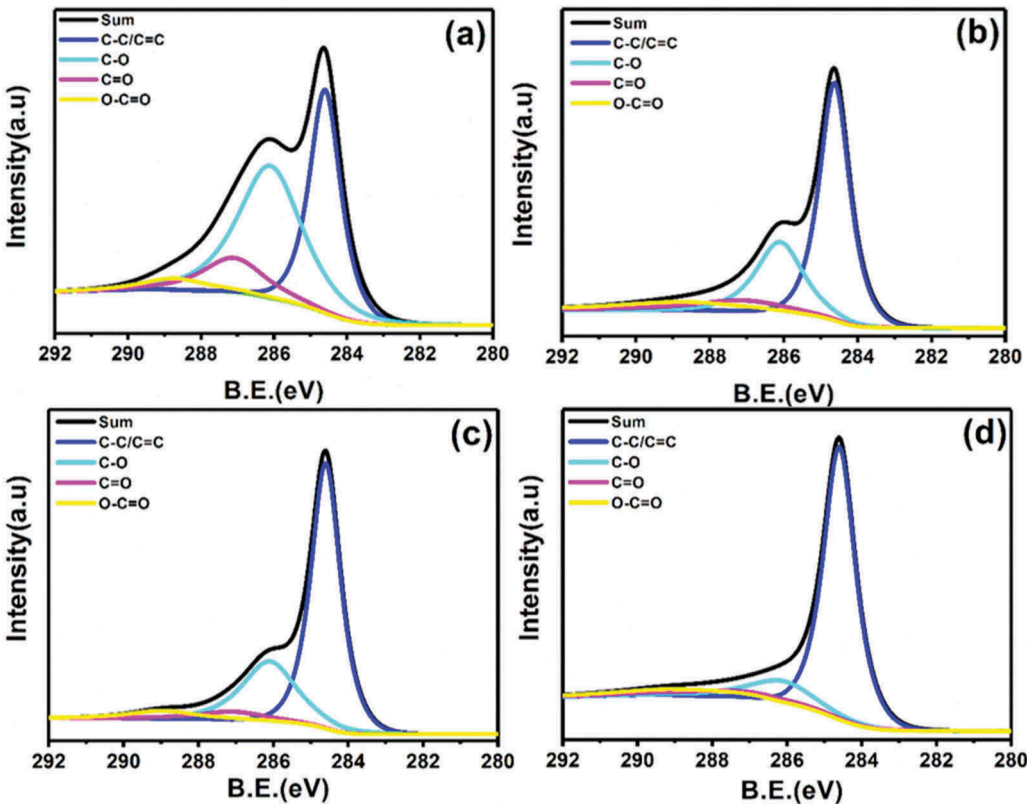

Figure 2. C1s XPS spectra of (a) GO, (b) 3h-RGO, (c) 5h-RGO and (d) 7h-RGO.

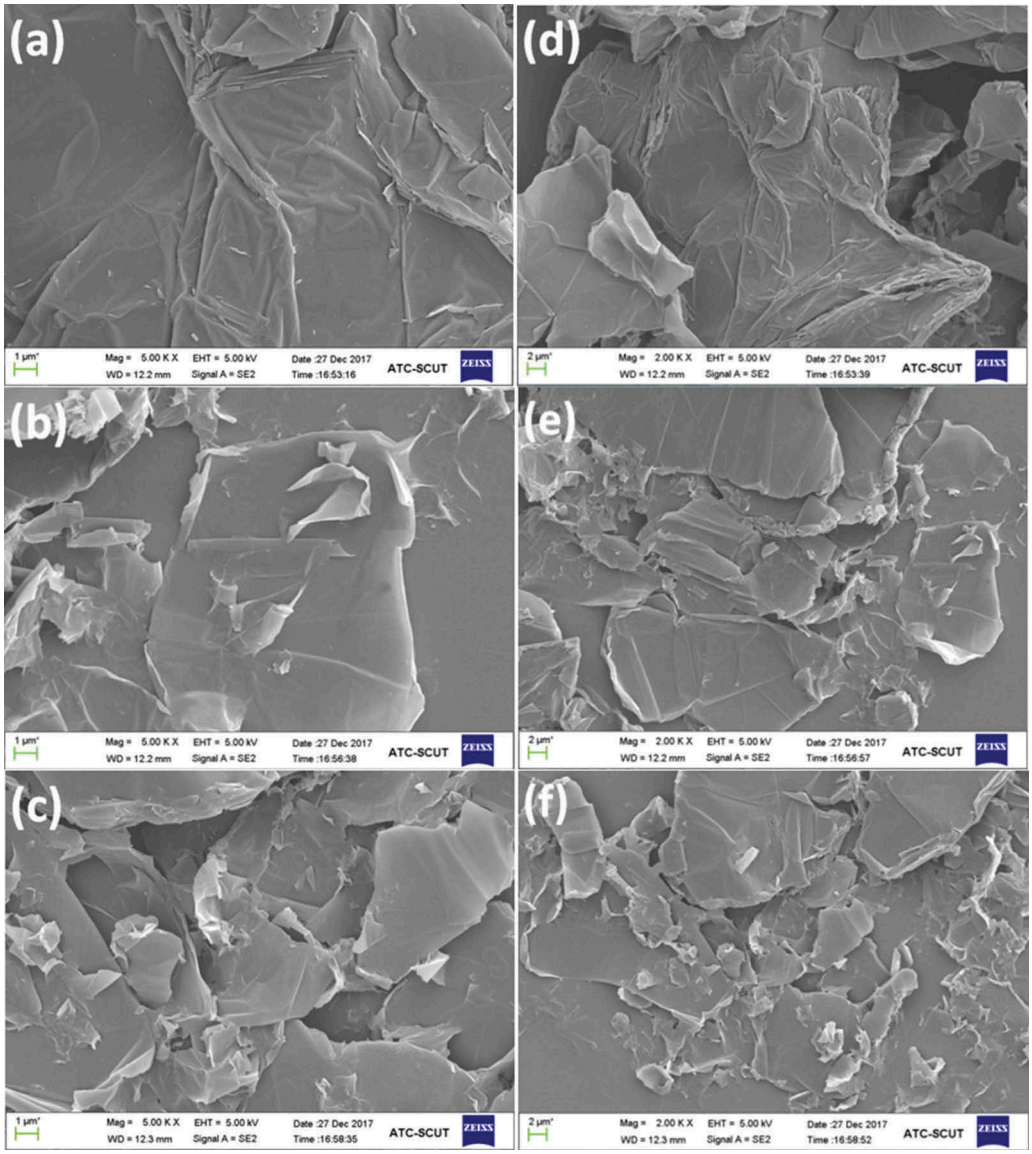

Figure 3. SEM images of (a) and (d) 3h-RGO; (b) and (e) 5h-RGO; (c) and (f) 7h-RGO.

as shown in Figure 4b, Red arrows are used to indicate the large and dark areas resulted from stacked graphene sheets in the matrix because of nanometer effect. Even though there exists little agglomeration in NBR, a good dispersion in large scale could be achieved, as shown in Figure 4c, which is beneficial for the absorption and mechanical properties.[36,37]

3.3. EM dielectric properties of RGO/NBR composites

EM parameters of RGO/NBR composites with different reduction time were measured by vector network analyzer using waveguide method. Figure 5 exhibits the real part (ε') and imaginary part (ε") of relative complex permittivity ($\varepsilon_r = \varepsilon'\text{-}i\varepsilon''$) in 26.5–40 GHz, which represent the storage ability and the attenuation capacity of EM absorbing materials, respectively.[35] As an EM transparent material, NBR showed very low and constant ε' and ε" values over the whole frequency band.[26] Besides, both RGO and NBR hold very low permeability in real part and imaginary part due to the weak magnetic characteristic. Therefore, only the ε' and ε" of the composites are displayed here. As shown in Figure 5, the value of ε' of 3h-RGO/NBR, 5h-RGO/NBR and 7h-RGO/NBR increased with increasing frequency, while the value of ε" decreases in the beginning and then increases gradually. The increase of ε' resulted from the Maxwell-Wagner polarization effect,[38] that was, the electrolytic polarization caused by charge accumulation would improve the value of ε'. The

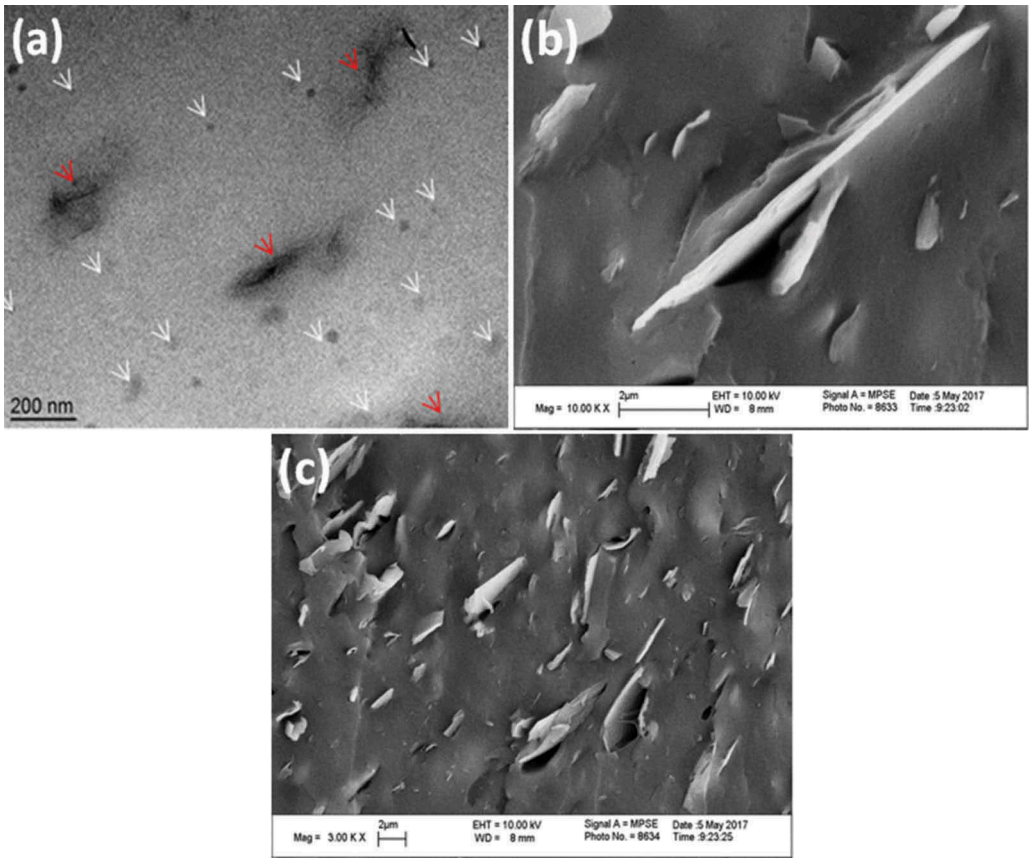

Figure 4. (a) TEM, (b) and (c) SEM micrographs of the 7h-RGO/NBR.

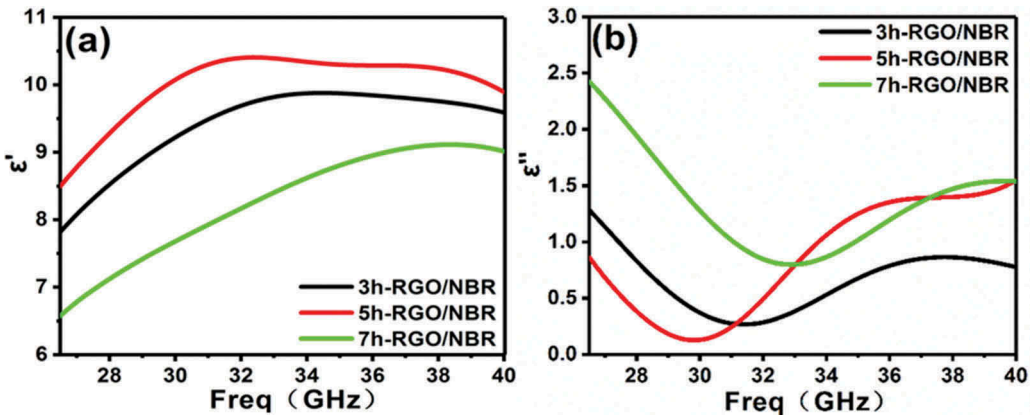

Figure 5. (a) Real part and (b) imaginary part of the complex permittivity of RGO/NBR composites.

decrease of ε" might be related to the resonance behavior.[25] Furthermore, the ε' of samples show a decreasing trend in the order from 5, 3 to 7 h, indicating different electrical conductivity of samples, which is generally affected by the residual oxygenic groups, structural integrity as well as the dispersion in matrix of graphene sheets.[39] It also could be noticed that the ε" of RGO/NBR composites decreased gradually from 7, 3 to 5 h in 26.5–31 GHz, but also decreased from 7, 5 to 3 h in 31–40 GHz. This result is presumably caused by the combined effect of conduction loss and relaxation loss, which fluctuate with the frequency. In addition, the relative complex permittivity of RGO/NBR composites with different reduction time keeps at a low value in the whole measured band, which helps to

reduce the reflection and enhance the absorption of incident wave for a better impedance match.

3.4. EM wave absorbing abilities of RGO/NBR composites

The EM wave RL value of RGO/NBR composites were calculated by the measured complex relative permittivity and permeability in 26.5–40 GHz at given sample thickness using Equation (1).[40]

$$RL = 20\lg\left|\frac{\sqrt{\frac{\mu_r}{\varepsilon_r}}\tanh\left(j\frac{2\pi fd}{c}\right)\sqrt{\varepsilon_r\mu_r}-1}{\sqrt{\frac{\mu_r}{\varepsilon_r}}\tanh\left(j\frac{2\pi fd}{c}\right)\sqrt{\varepsilon_r\mu_r}+1}\right| \quad (1)$$

where ε_r and μ_r are the complex relative permittivity and permeability, respectively, c is the velocity of light in vacuum, d is the absorber thickness, and f is the frequency. Calculated RL curves of composites are given in Figure 6. It could be observed that the RGO/NBR composites exhibit excellent microwave absorbing properties in measured region, with low reflection loss and wide effective absorption bandwidth (<-10 dB). Among all samples, 3h-RGO/NBR shows the best performance for the minimum RL of −45 dB at only 2.1 mm and 5 GHz bandwidth of RL below −10 dB at all thicknesses apart from 2.5 mm. Furthermore, the RL values exceed −20 dB at all thicknesses of 2.0–2.4 mm. For 5h-RGO/NBR, it reaches the RL value below −15 dB and effective bandwidth (<-10 dB) beyond 4 GHz at 2.0–2.5 mm. It also reaches the minimum RL of −42.5 dB at the thickness of 2.5 mm, where the bandwidth of RL value below −10 dB is just 4 GHz. In addition, the effective bandwidth of 5h-RGO/NBR at 2.3 and 2.4 mm is up to 6 GHz. 7h-RGO/NBR shows similar absorbing characteristic as 5-RGO/NBR for reaching the RL value below −15 dB at all thicknesses. Better yet, it shows a wider effective bandwidth (<-10 dB) of 6.5 GHz at all thicknesses apart from 2.5 mm, where the −10 dB absorption frequency band is only 5 GHz but the minimum RL is −38.5 dB. In addition to the reduction time, it is noteworthy that thickness of samples also have great influence on the microwave absorbing property. The frequency corresponding to the minimum RL value would shift towards lower values with increasing thickness.[4,5] Table 2 summarized the recent reported materials that could be used in 5G. Compared with obvious materials, the absorbing property of RGO/NBR composites obtained in this work is obviously excellent in many ways, such as better deformability, lower absorbent content and stronger absorbing ability over wide frequency band.

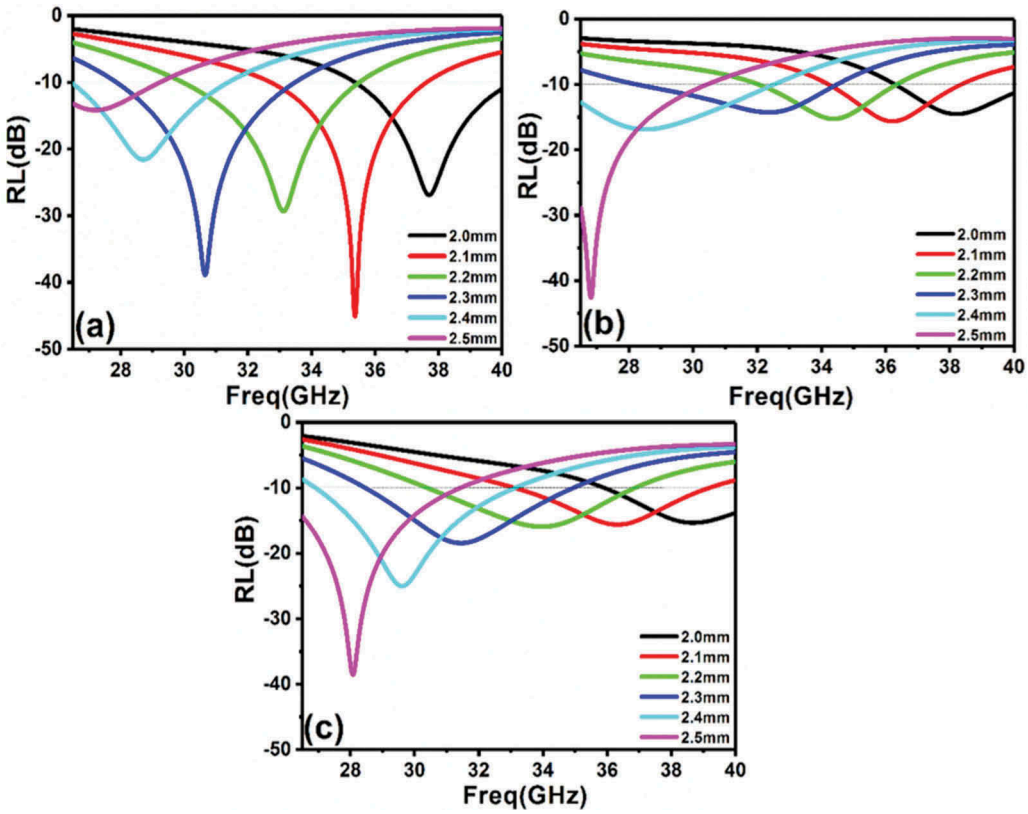

Figure 6. RL curves for RGO/NBR composites of different reduction time in the frequency range of 26.5–40 GHz (a) 3h-RGO/NBR, (b) 5h-RGO/NBR and (c)7h-RGO/NBR.

Table 2. Existing EM wave absorbing materials that can be used in 5G. Abbreviations: BaM, $BaFe_{12}O_{19}$; MEG, magnetic expanded graphite; CIP, carbonyl-iron powder.

Samples	Matrix	Optimal Thickness	Concentration	RL_{min} (dB)	Frequency below −10 dB (GHz)	Ref
(BaM+ $BaTiO_3$)/Polyaniline	Epoxy Resin	2 mm	66 wt %	−22	34.5–37.5	[41]
ZnO Whisker	Silicon Resin	2 mm	50 wt%	−14	66–78	[42]
MEG/CIP	Silicone Rubber	1.5 mm	3 mg/cm^3	−10.8	32–38	[43]
ε-$Ga_xFe_{x-2}O_3$	/	217.2 μm	100 wt%	−215	58–62	[44]
3h-RGO	NBR	2.1 mm	10 wt%	−45	32.6–37.6	This work
5h-RGO	NBR	2.5 mm	10 wt%	−42.5	26.5–30.5	This work
7h-RGO	NBR	2.5 mm	10 wt%	−38.5	26.5–31.5	This work

It is well known that impedance match and electromagnetic attenuation are two basic principles of microwave absorbing materials.[43] Low complex permittivity of RGO/NBR composites leads to a weak reflection of incident EM wave and provides proper impedance, which are beneficial to achieve strong microwave absorption property. The EM attenuation capability of RGO/NBR composites is determined by many factors. The first is the conduction loss, which comes from an oscillatory current induced by the directional motion of carrier charges, appearing in all RGO/NBR composites. The second one is polarization from lattice imperfections and residual oxygen-containing groups of graphene sheets, which act as the polarization centers and arouse the localized states near Fermi level, where the EM energy could be dissipated by the transition from contiguous states to Fermi level in alternative EM field. The third way is relaxation effect, which include the dielectric relaxation caused by the lag of induced charges, the polarization relaxation from structure defect and the electric dipole polarization resulted from the different ability of C and O in residual oxidized functional groups to catch electrons.[38] Beyond above conventional loss mechanism, the interface scattering and multiple reflections also play critical role in attenuating microwave. The numerous interfaces of RGO and NBR could lengthen the spread road of incident wave and contribute to the final absorption of EM wave.[26]

For 3h-RGO/NBR, the strongest absorption could be ascribed to two main reasons. One is the most oxidized functional groups, which arouse much electric dipole polarization. The other is the most complete graphene sheets that could provide strong multiple interface reflection by forming dihedral angle, just as reported by Vivek K. Singh.[26] Compared with 5h-RGO/NBR, 7h-RGO/NBR has the similar reduction degree but stronger absorbing ability and wider effective bandwidth, which may be ascribed to the stronger polarization relaxation due to more structure defect caused by longer reduction

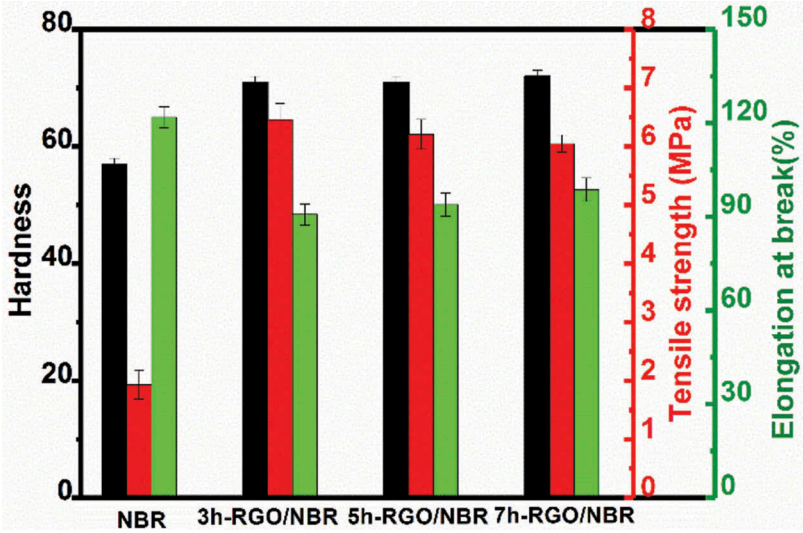

Figure 7. Mechanical properties of (a) neat NBR, (b) 3h-RGO/NBR, (c) 5h-RGO/NBR and (d) 7h-RGO/NBR.

time. In addition, the tiny otherness in impedance match also contributed to the performance difference.

3.5. Mechanical properties

As structural absorbing materials, RGO/NBR composites should have not only strong absorbing ability, but also outstanding mechanical properties. To clearly visualize the mechanical properties of the prepared composites, the shore A hardness, tensile strength and elongation at break of neat NBR and RGO/NBR composites were tested and given in Figure 7. It could be seen that shore A hardness of neat NBR is 57, while that of RGO/NBR composites with different reduction time are 71, 71 and 72, respectively. The tensile strength of composites also exhibits a significant increase of more than 3 times compared with neat NBR, while the elongation at break slightly decreased accordingly, which is due to the enhancement effect of RGO and its uniform dispersion in NBR matrix.[45] All composites show similar mechanical properties, which demonstrates a modest effect from reduction time. Good mechanical property would endow RGO/NBR absorbing rubber great potential in broader applications.

4. Conclusions

In summary, RGO/NBR composites with different reduction time of 3, 5 and 7 h were prepared in this study. The correlation among reduction time, structure and absorption property in 26.5–40 GHz of samples were discussed in detail through various characterizations. Compared with existing EM wave absorbing materials that could be used in 5G, RGO/NBR composites obtained in this study exhibit better absorbing ability in 26.5–40 GHz by achieving the minimum RL value of −45 dB at 35.4 GHz and 6.5 GHz effective bandwidth with only 2.1 mm. Besides, they also possess outstanding mechanical properties. Therefore, RGO/NBR composites could hopefully be used as ideal candidate of millimeter wave absorbing materials for 5G applications.

The microwave absorption abilities of RGO/NBR composites, which were arguably derived from conduction loss, polarization relaxation and multiple interface reflections, were found to be strongly associated with thickness and reduction time for its determined role in reduction degree and structure of graphene sheets. Therefore, the microwave absorption ability of composites could be well regulated by changing reduction time and sample thickness, which make it easy to customize optimal electromagnetic absorption material for specific requirement. Besides the above mentioned factors, the grain size of RGO and its dispersion in NBR are presumably influence factors to affect the EM wave absorption, and more detailed studies will be conducted later.

Funding

This work was supported by the Program of Guangdong Provincial Department of Science and Technology [2016A010103004];Fundamental Research Funds for the Central Universities;Program of Guangzhou Science Technology and Innovation Commission [201607010103].

References

[1] Kong, L.; Yin, X. W.; Yuan, X. Y.; Zhang, Y. J.; Liu, X. M.; Cheng, L. F.; Zhang, L. T., Electromagnetic Wave Absorption Properties of Graphene Modified with Carbon Nanotube/Poly(Dimethyl Siloxane) Composites. *Carbon*. **2014**, *73*, 185–193. DOI: 10.1016/j.carbon.2014.02.054.

[2] Chen, D. Z.; Wang, G. S.; He, S.; Liu, J.; Guo, L.; Cao, M. S., Controllable Fabrication of Mono-Dispersed RGO-hematite Nanocomposites and Their Enhanced Wave Absorption Properties. *J. Mater. Chem. A*. **2013**, *1*, 5996–6003. DOI: 10.1039/c3ta10664k.

[3] Liu, J. W.; Che, R. C.; Chen, H. J.; Zhang, F.; Feng, X.; Wu, Q. S.; Wang, M., Microwave Absorption Enhancement of Multifunctional Composite Microspheres with Spinel Fe_3O_4 Cores and Anatase TiO_2 Shells. *Small*. **2012**, *8*, 1214–1221. DOI: 10.1002/smll.201102245.

[4] Wang, L. N.; Jia, X. L.; Li, Y. F.; Yang, F.; Zhang, L. Q.; Liu, L. P.; Ren, X.; Yang, H. T., Synthesis and Microwave Absorption Property of Flexible Magnetic Film Based on Graphene Oxide/Carbon Nanotubes and Fe3O4 Nanoparticles. *J. Mater. Chem. A*. **2014**, *2*, 14940–14946. DOI: 10.1039/c4ta02815e.

[5] Li, X. H.; Feng, J.; Du, Y. P.; Bai, J. T.; Fan, H. M.; Zhang, H. L.; Peng, Y.; Li, F. S., One-Pot Synthesis of $CoFe_2O_4$/graphene Oxide Hybrids and Their Conversion into FeCo/graphene Hybrids for Lightweight and Highly Efficient Microwave Absorber. *J. Mater. Chem. A*. **2015**, *3*, 5535–5546. DOI: 10.1039/c4ta05718j.

[6] European Commission. Opinion on a Long-Term Strategy on Future Spectrum Needs and Use of Wireless Audio and Video PMSE Applications. RSPG17-037 FINAL REV1, Brussels. Accessed on 21 November 2017. http://ec.europa.eu/eurostat/news/news-releases.

[7] Zhang, X. J.; Wang, G. S.; Wei, Y. Z.; Guo, L.; Cao, M. S., Polymer-Composite with High Dielectric Constant and Enhanced Absorption Properties Based on graphene-CuS Nanocomposites and Polyvinylidene Fluoride. *J. Mater. Chem. A*. **2013**, *1*, 12115–12122. DOI: 10.1039/c3ta12451g.

[8] Cho, H. S.; Kim, S. S., Design of Grid-Type Microwave Absorbers with High-Permittivity Composites of

Ag-Coated Ni-Zn Ferrite Particles. *J. Appl. Phys.* **2015**, *117*, 17A31. DOI: 10.1063/1.4913645.

[9] Liu, P. B.; Huang, Y.; Zhang, X., Synthesis and Excellent Microwave Absorption Properties of Graphene/Polypyrrole Composites with Fe_3O_4 Particles Prepared via a Co-Precipitation Method. *Mater. Lett.* **2014**, *129*, 35–38. DOI: 10.1016/j.matlet.2014.04.194.

[10] Cao, L. M.; Yuan, D. S.; Xu, C. H.; Chen, Y. K., Biobased, Self-Healable, High Strength Rubber with Tunicate Cellulose Nanocrystals. *Nanoscale*. **2017**, *9*, 15696–15706. DOI: 10.1039/c7nr05011a.

[11] Saini, L.; Barala, S. K.; Patra, M. K.; Jani, R. K.; Dixit, A.; Vadera, S. R., Ferroelectrically Induced Dual Band Microwave Absorption in Multiferroic $BiFeO_3$/acrylo-nitrile Butadiene Rubber Composites. *Appl. Phys. A*. **2017**, *123*, 685. DOI: 10.1007/s00339-017-1323-5.

[12] Cao, L. M.; Fu, X. F.; Xu, C. H.; Yin, S. H.; Chen, Y. K. High-Performance Natural Rubber Nanocomposites with Marine Biomass (Tunicate Cellulose). *Cellulose*. **2017**, *24*, 1–12. DOI: 10.1007/s10570-017-1293-y.

[13] Xu, C. H.; Cao, L. M.; Huang, X. H.; Chen, Y. K.; Lin, B. F.; Fu, L. H., Self-Healing Natural Rubber with Tailorable Mechanical Properties Based on Ionic Supramolecular Hybrid Network. *ACS Appl. Mater. Inter.* **2017**, *9*, 29363–29373. DOI: 10.1021/acsami.7b09997.

[14] Xu, C. H.; Cao, L. M.; Lin, B. F.; Liang, X. Q.; Chen, Y. K., Design of Self-Healing Supramolecular Rubbers by Introducing Ionic Cross-Links into Natural Rubber via a Controlled Vulcanization. *ACS Appl. Mater. Inter.* **2016**, *8*, 17728–17737. DOI: 10.1021/acsami.6b05941.

[15] Wang, G. Z.; Peng, X. G.; Yu, L.; Wan, G. P.; Lin, S. W.; Qin, Y., Enhanced Microwave Absorption of ZnO Coated with Ni Nanoparticles Produced by Atomic Layer Deposition. *J. Mater. Chem. A*. **2015**, *3*, 2734–2740. DOI: 10.1039/c4ta06053a.

[16] Xia, F.; Liu, J. W.; Gu, D.; Zhao, P. F.; Zhang, J.; Che, R. C., Microwave Absorption Enhancement and Electron Microscopy Characterization of $BaTiO_3$ Nano-Torus. *Nanoscale*. **2011**, *3*, 3860–3867. DOI: 10.1039/c1nr10606f.

[17] Yang, H. B.; Ye, T.; Lin, Y.; Liu, M.; Zhang, G.; Kang, P., Giant Enhancement of $(Bh)_{Max}$ in $BaFe_{12}O_{19}/Y_3Fe_5O_{12}$ Nanocomposite Powders. *Mater. Lett.* **2015**, *145*, 19–22. DOI: 10.1016/j.matlet.2015.01.080.

[18] You, W. B.; Bi, H.; She, W.; Zhang, Y.; Che, R. C., Dipolar-Distribution Cavity γ-Fe_2O_3@C@α-MnO_2 Nanospindle with Broadened Microwave Absorption Bandwidth by Chemically Etching. *Small*. **2017**, *13*, 1602779. DOI: 10.1002/smll.201602779.

[19] Wang, G. Z.; Gao, Z.; Tang, S. W.; Chen, C. Q.; Duan, F. F.; Zhao, S. C.; Lin, S. W.; Feng, Y. H.; Zhou, L.; Qin, Y., Microwave Absorption Properties of Carbon Nanocoils Coated with Highly Controlled Magnetic Materials by Atomic Layer Deposition. *ACS Nano*. **2012**, *6*, 11009–11017. DOI: 10.1021/nn304630h.

[20] Zhang, Y. C.; Liu, Y.; Wang, X.; Yuan, Y. H.; Lai, W. C.; Wang, Z. M.; Zhang, X. J.; Liu, X. Y., Towards Efficient Microwave Absorption: Intrinsic Heterostructure of Fluorinated SWCNT. *J. Mater. Chem. C*. **2017**, *5*, 11847–11855. DOI: 10.1039/c7tc04141a.

[21] Zhai, Y.; Zhang, Y.; Ren, W., Electromagnetic Characteristic and Microwave Absorbing Performance of Different Carbon-Based Hydrogenated Acrylonitrile–Butadiene Rubber Composites. *Mater. Chem. Phys.* **2012**, *133*, 176–181. DOI: 10.1016/j.matchemphys.2012.01.004.

[22] Flaifel, M. H.; Ahmad, S. H.; Abdullah, M. H.; Rasid, R.; Shaari, A. H.; El-Saleh, A. A.; Appadu, S., Preparation, Thermal, Magnetic and Microwave Absorption Properties of Thermoplastic Natural Rubber Matrix Impregnated with NiZn Ferrite Nanoparticles. *Compos. Sci. Technol.* **2014**, *96*, 103–108. DOI: 10.1016/j.compscitech.2014.03.016.

[23] Vinayasree, S.; Soloman, M. A.; Sunny, V.; Mohanan, P.; Kurian, P.; Joy, P. A.; Anantharaman, M. R., Flexible Microwave Absorbers Based on Barium Hexaferrite, Carbon Black, and Nitrile Rubber for 2-12 GHz Applications. *J. Appl. Phys.* **2014**, *116*, 024902. DOI: 10.1063/1.4886382.

[24] Vinayasree, S.; Soloman, M. A.; Sunny, V.; Mohanan, P.; Kurian, P.; Anantharaman, M. R., A Microwave Absorber Based on Strontium Ferrite-Carbon Black-Nitrile Rubber for S and X-Band Applications. *Compos. Sci.Technol.* **2013**, *82*, 69–75. DOI: 10.1016/j.compscitech.2013.04.010.

[25] Al-Ghamdi, A. A.; Al-Ghamdi, A. A.; Al-Turki, Y.; Yakuphanoglu, F.; El-Tantawy, F., Electromagnetic Shielding Properties of Graphene/Acrylonitrile Butadiene Rubber Nanocomposites for Portable and Flexible Electronic Devices. *Composites Part. B Eng.* **2016**, *88*, 212–219. DOI: 10.1016/j.compositesb.2015.11.010.

[26] Singh, V. K.; Shukla, A.; Patra, M. K.; Saini, L.; Jani, R. K.; Vadera, S. R.; Kumar, N., Microwave Absorbing Properties of a Thermally Reduced Graphene Oxide/Nitrile Butadiene Rubber Composite. *Carbon*. **2012**, *50*, 2202–2208. DOI: 10.1016/j.carbon.2012.01.033.

[27] Wu, J. L.; Shen, X. P.; Lei, J.; Wang, K.; Chen, K. M., Solvothermal Synthesis and Characterization of Sandwich-Like graphene/ZnO Nanocomposites. *Appl. Surf. Sci.* **2010**, *256*, 2826–2830. DOI: 10.1016/j.apsusc.2009.11.034.

[28] Meriga, V.; Valligatla, S.; Sundaresan, S.; Cahill, C.; Dhanak, V. R.; Chakraborty, A. K., Optical, Electrical, and Electrochemical Properties of Graphene Based Water Soluble Polyaniline Composites. *J. Appl. Polym. Sci.* **2015**, *132*, 42766. DOI: 10.1002/app.42766.

[29] Cançado, L. G.; Jorio, A.; Ferreira, E. H. M.; Stavale, F.; Achete, C. A.; Capaz, R. B.; Moutinho, M. V. O.; Lombardo, A.; Kulmala, T. S.; Ferrari, A. C., Quantifying Defects in Graphene via Raman Spectroscopy at Different Excitation Energies. *Nano Lett.* **2011**, *11*, 3190–3196. DOI: 10.1021/nl201432g.

[30] Liu, W. W.; Li, H.; Zeng, Q. P.; Duan, H. N.; Guo, Y. P.; Liu, X. F.; Sun, C. Y.; Liu, H. Z., Fabrication of Ultralight Three-Dimensional Graphene Networks with Strong Electromagnetic Wave Absorption Properties. *J. Mater. Chem. A*. **2015**, *3*, 3739–3747. DOI: 10.1039/c4ta06091a.

[31] Kuang, B. Y.; Song, W. L.; Ning, M. Q.; Li, J. B.; Zhao, Z. J.; Guo, D. Y.; Cao, M. S.; Jin, H. B., Chemical Reduction Dependent Dielectric Properties and Dielectric Loss Mechanism of Reduced Graphene Oxide. *Carbon*. **2017**, *127*, 209–217. DOI: 10.1016/j.carbon.2017.10.092.

[32] Kumar, R.; Khan, S.; Gupta, N.; Naqvi, S.; Gaurav, K.; Sharma, C.; Kumar, M.; Kumar, P.; Chand, S., Fullerene Grafted Graphene Oxide with Effective Charge Transfer Interactions. *Carbon*. **2016**, *107*, 765–773. DOI: 10.1016/j.carbon.2016.06.034.

[33] Narayan, R.; Lim, J.; Jeon, T.; Dong, J. L.; Sang, O. K., Perylene Tetracarboxylate Surfactant Assisted Liquid Phase Exfoliation of Graphite into Graphene Nanosheets with Facile Re-Dispersibility in Aqueous/Organic Polar Solvents. *Carbon*. **2017**, *119*, 555–568. DOI: 10.1016/j.carbon.2017.04.071.

[34] Park, S.; An, J.; Potts, J. R.; Velamakanni, A.; Murali, S.; Ruoff, R. S., Hydrazine-Reduction of Graphite- and Graphene Oxide. *Carbon*. **2011**, *49*, 3019–3023. DOI: 10.1016/j.carbon.2011.02.071.

[35] Zhang, X. J.; Wang, G. S.; Cao, W. Q.; Wei, Y. Z.; Liang, J. F.; Guo, L.; Cao, M. S., Enhanced Microwave Absorption Property of Reduced Graphene Oxide (Rgo)-$Mnfe_2o_4$ Nanocomposites and Polyvinylidene Fluoride. *ACS Appl. Mater. Inter*. **2014**, *6*, 7471–7478. DOI: 10.1021/am500862g.

[36] Xu, C. H.; Cui, R.; Fu, L. H.; Lin, B. F., Recyclable and Heat-Healable Epoxidized Natural Rubber/bentonite Composites. *Compos. Sci.technol.* **2018**, *167*, 421-430. DOI: 10.1016/j.compscitech.2018.08.027

[37] Gan, L.; Dong, M.; Han, Y.; Xie, X. F.; Yang, L.; Huang, J., Connection-Improved Conductive Network Of Carbon Nanotubes in a Rubber Cross-Link Network. Acs Appl. Mater. Sci. Interfaces **2018**, *10*, 18213-18219. DOI: 10.1021/acsami.8b03081

[38] Wang, C.; Han, X. J.; Xu, P.; Zhang, X. L.; Du, Y. C.; Hu, S. R.; Wang, J. Y.; Wang, X. H., The Electromagnetic Property of Chemically Reduced Graphene Oxide and Its Application as Microwave Absorbing Material. *Appl. Phys. Lett*. **2011**, *98*, 072906. DOI: 10.1063/1.3555436.

[39] Gong, L. X.; Zhao, L.; Tang, L. C.; Liu, H. Y.; Mai, Y. W., Balanced Electrical, Thermal and Mechanical Properties of Epoxy Composites Filled with Chemically Reduced Graphene Oxide and Rubber Nanoparticles. *Compos. Sci.Technol*. **2015**, *121*, 104–114. DOI: 10.1016/j.compscitech.2015.10.023.

[40] Yang, C. C.; Gung, Y. J.; Shih, C. C.; Hung, W. C.; Wu, K. H., Synthesis, Infrared and Microwave Absorbing Properties of ($Bafe_{12}o_{19}$+$Batio_3$) /Polyaniline Composite. *J. Magn. Magn. Mater*. **2011**, *323*, 933–938. DOI: 10.1016/j.jmmm.2010.11.072.

[41] Hung, W. C.; Cheng, K. F.; Lan, C. H.; Chang, Y. C.; Wu, K. H., Preparation and Infrared/Millimeter Wave Attenuation Properties of Magnetic Expanded Graphite by Explosive Combustion. *Mater. Express*. **2016**, *6*, 53–60. DOI: 10.1166/mex.2016.1282.

[42] Namai, A.; Kurahashi, S.; Goto, T.; Ohkoshi, S. I., Theoretical Design of a High-Frequency Millimeter Wave Absorbing Sheet Composed of Gallium Substituted ε-Fe_2O_3 Nanomagnet. *IEEE Trans. Magn*. **2012**, *48*, 4386–4389. DOI: 10.1109/TMAG.2012.2199091.

[43] Yang, R. B.; Kuo, W. S.; Lai, H. C., Effect of Carbon Nanotube Dispersion on the Complex Permittivity and Absorption of Nanocomposites in 2-18 GHz Ranges. *J. Appl. Polym. Sci*. **2014**, *131*, 8558–8572. DOI: 10.1002/app.40963.

[44] Zhang, S. Y.; Cao, Q. X.; Xue, Y. R.; Zhou, Y. X., Microwave Absorption Performance of the Absorber Based on epsilon-Fe_3N/epoxy and Carbonyl Iron/Epoxy Composites. *J. Magn. Magn. Mater*. **2015**, *374*, 755–761. DOI: 10.1016/j.jmmm.2014.08.073.

[45] Xu, C. H.; Nie, J. D.; Wu, W. C.; Fu, L. H.; Lin, B. F., Design of Self-Healable Supramolecular Hybrid Network Based on Carboxylated Styrene Butadiene Rubber and Nano-Chitosan. Carbohyd. Polym. **2018**, DOI: 10.1016/j.carbpol.2018.10.080

[46] Xuan, X.; Zhang, H. Y.; Zeng, G. X.; Bo, N. K.; Chan, C. H., Millimeter Wave Absorbing Electromagnetic Properties of ZnO Whisker/Silicon Resin Coating Material. *Mater. Sci. Forum*. **2016**, *852*, 1055–1059. DOI: 10.4028/www.scientific.net/MSF.852.1055.